Supporting Information:

Following *in Situ* the Deposition of Gold Electrodes on Low Band Gap Polymer Films

*Franziska C. Löhrer[†], Volker Körstgens[†], Gabriele Semino[†], Matthias Schwartzkopf[‡], Alexander Hinz[§], Oleksandr Polonskyi[§], Thomas Strunskus[§], Franz Faupel[§], Stephan V. Roth[‡,⊥], and Peter Müller-Buschbaum[†,∥,]**

[†] Physik-Department, Lehrstuhl für Funktionelle Materialien, Technische Universität München, James-Franck-Str. 1, 85748 Garching, Germany

[‡] Deutsches Elektronen-Synchrotron (DESY), Notkestrasse 85, 22607 Hamburg, Germany

[§] Institut für Materialwissenschaft, Lehrstuhl für Materialverbunde, Christian-Albrechts-Universität zu Kiel, Kaiserstraße 2, 24143 Kiel, Germany

[⊥] Department of Fiber and Polymer Technology, KTH Royal Institute of Technology, Teknikringen 56-58, 10044 Stockholm, Sweden

[∥] Heinz Maier-Leibnitz-Zentrum, Lichtenbergstr. 1, 85748 Garching, Germany

* corresponding author E-Mail: muellerb@ph.tum.de

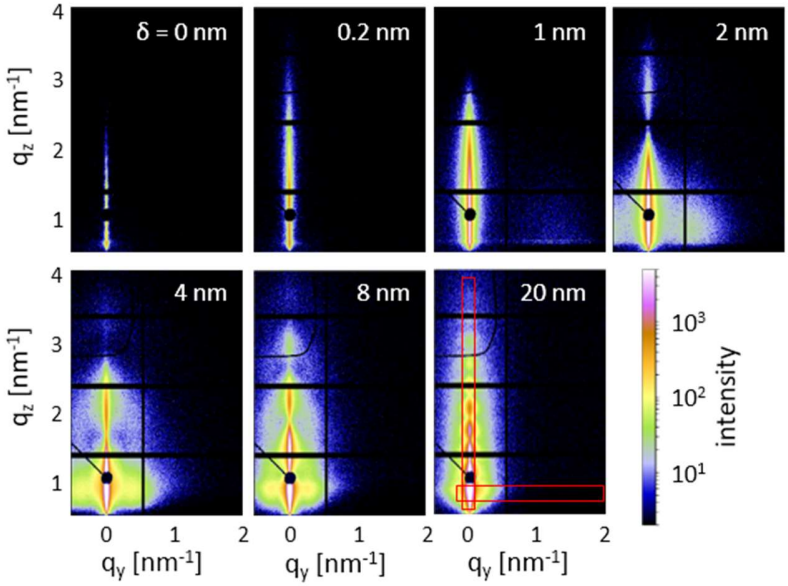

Figure S1: Exemplary 2D GISAXS data for PTB7 taken at specific points in time, corresponding to the pure polymer film (effective gold film thickness $\delta = 0$ nm), the five different growth phases ($\delta \approx 0.2$, 1, 2, 4, and 8 nm) as well as a late growth stage ($\delta \approx 20$ nm). In horizontal direction, the in-plane evolution of structures can be observed in form of intensity maxima, while in vertical direction, the formation of Kiessig fringes resulting from the gold layer is seen. The typical regions of interest (ROI) are shown in the last 2D image, with the vertical line cut integrated over 11 pixels and the horizontal line cut over 31 pixels of the 2D images.

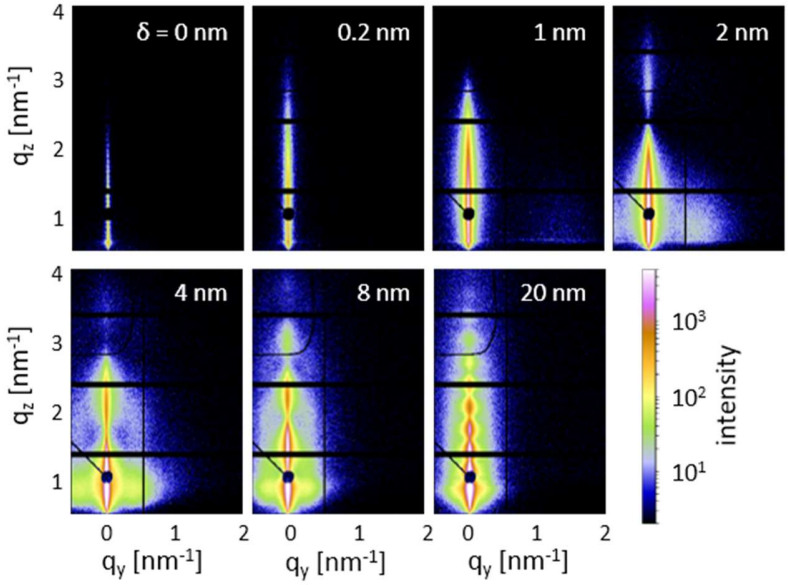

Figure S2: Exemplary 2D GISAXS data for PTB7-Th taken at specific points in time, corresponding to the pure polymer film (effective gold film thickness $\delta = 0$ nm), the five different growth phases ($\delta \approx 0.2$, 1, 2, 4, and 8 nm) as well as a late growth stage ($\delta \approx 20$ nm). In horizontal direction, the in-plane evolution of structures can be observed by intensity maxima, while in vertical direction, the formation of Kiessig fringes resulting from the gold layer is seen. The typical regions of interest (ROI) are shown in the last 2D image of Figure S1, with the vertical line cut integrated over 11 pixels and the horizontal line cut over 31 pixels of the 2D images.

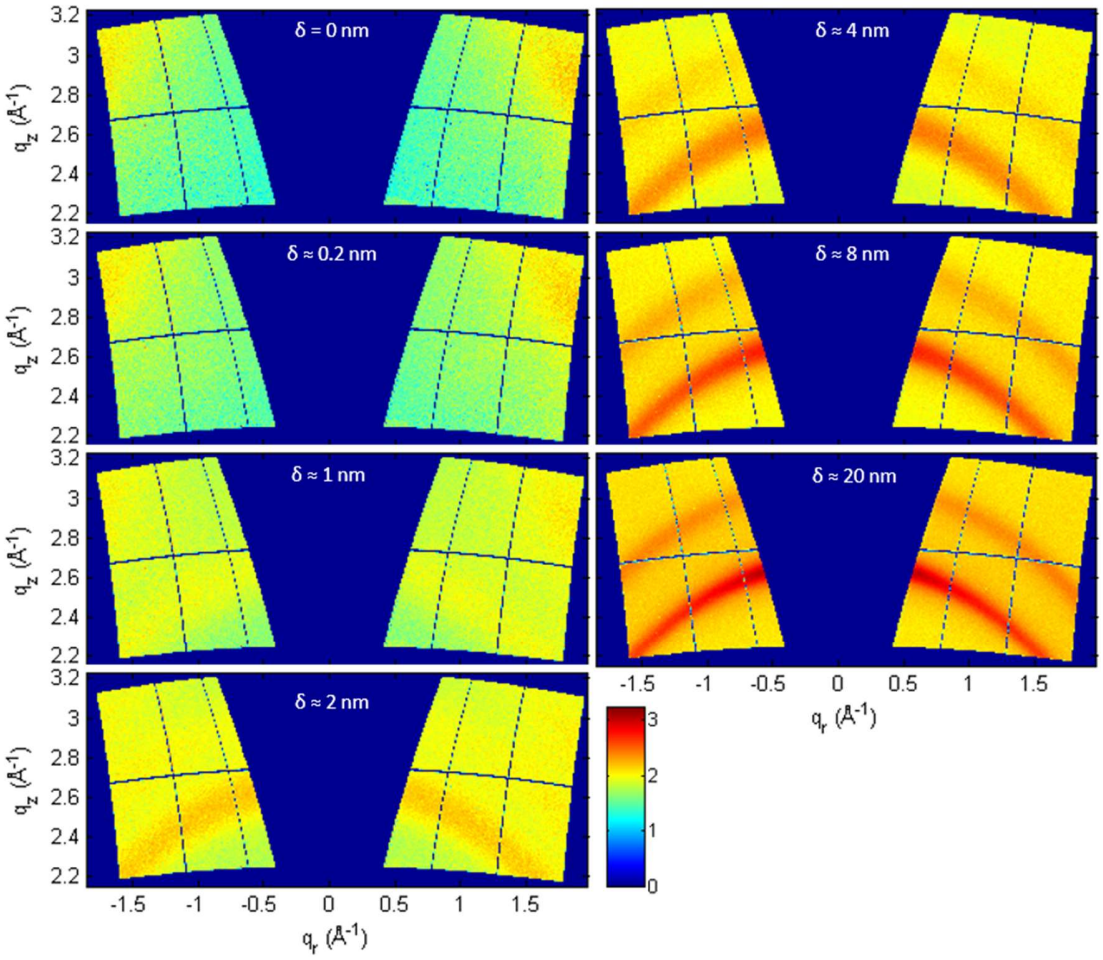

Figure S3: Exemplary 2D GIWAXS data for PTB7 taken at specific points in time, corresponding to the pure polymer film (effective gold film thickness $\delta = 0$ nm), the five different growth phases ($\delta \approx 0.2$, 1, 2, 4, and 8 nm) as well as a late growth stage ($\delta \approx 20$ nm). Vertical cake cuts were taken, as sketched in Figure S5, integrating over angles χ between -15 ° and +15 °. Intensity corrections and reshaping steps were performed using the MATLAB-based software GIXSGUI. (Jiang 2015)

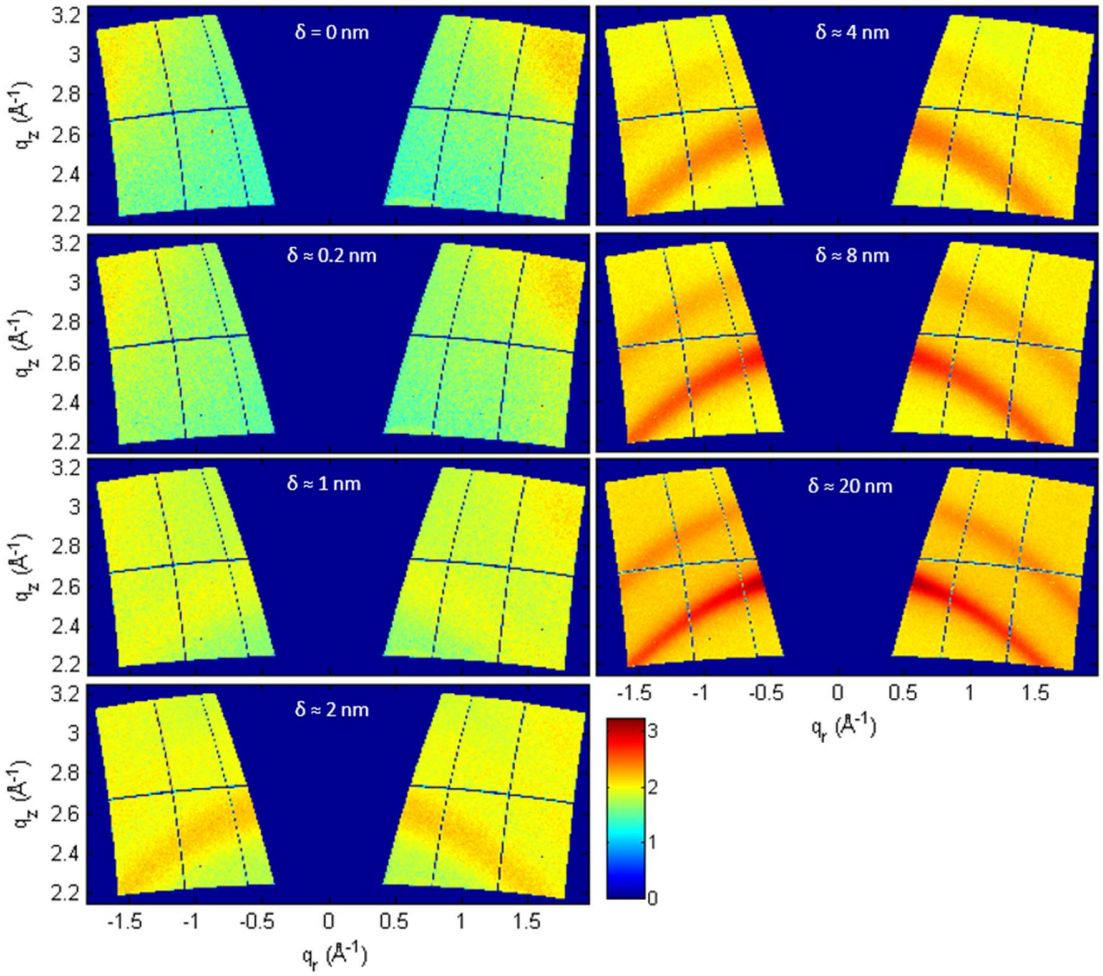

Figure S4: Exemplary 2D GIWAXS data for PTB7 taken at specific points in time, corresponding to the pure polymer film (effective gold film thickness $\delta = 0$ nm), the five different growth phases ($\delta \approx 0.2$, 1, 2, 4, and 8 nm) as well as a late growth stage ($\delta \approx 20$ nm). Vertical cake cuts were taken, as sketched in Figure S5, integrating over angles χ between -15 ° and +15 °. Intensity corrections and reshaping steps were performed using the MATLAB-based software GIXSGUI. (Jiang 2015)

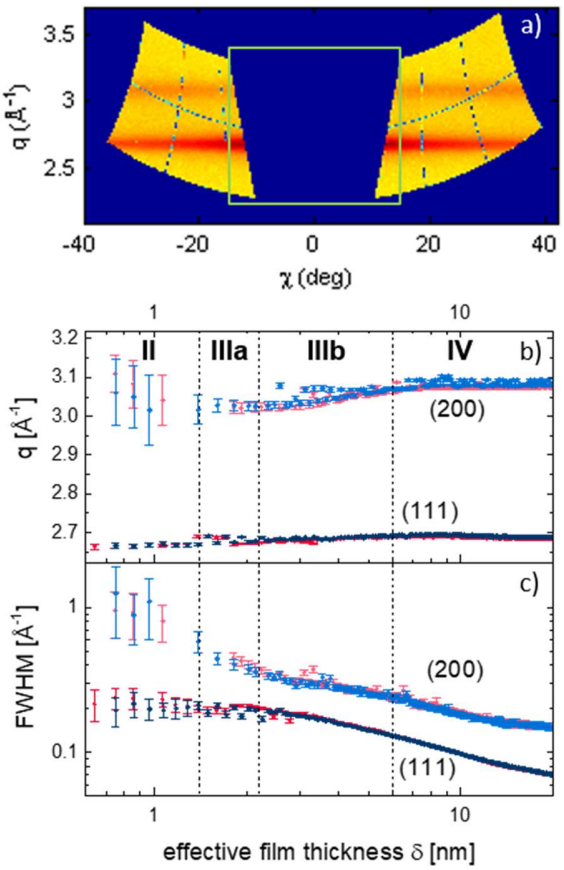

Figure S5: a) Exemplary region of interest for the vertical cuts shown in Figure 2 (for χ between -15° and 15°). The Bragg peaks (111) and (200) were fitted with Pseudo-Voigt functions plus constant background for all frames. The results are plotted over effective film thickness, showing no pronounced differences between the polymers. The b) q position is established after an effective film thickness of around $\delta \approx 3$ nm (111) and 4 nm (200), the c) FWHM exhibits an exponential decrease starting at $\delta \approx$ 2.3 nm (111) and 1 nm (200).

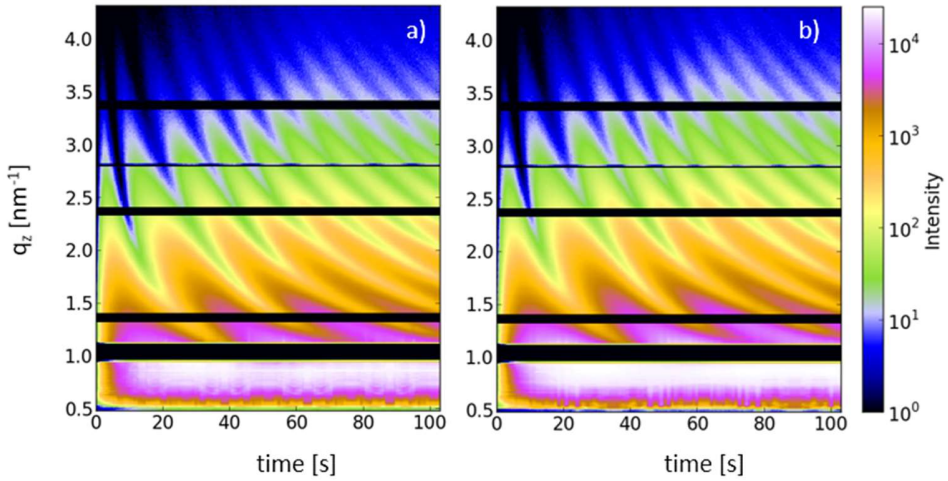

Figure S6: Contour mapping plots of the vertical line cuts (as indicated in Figure S1) integrated for every frame for a) PTB7 and b) PTB7-Th and plotted as a function of sputter deposition time.

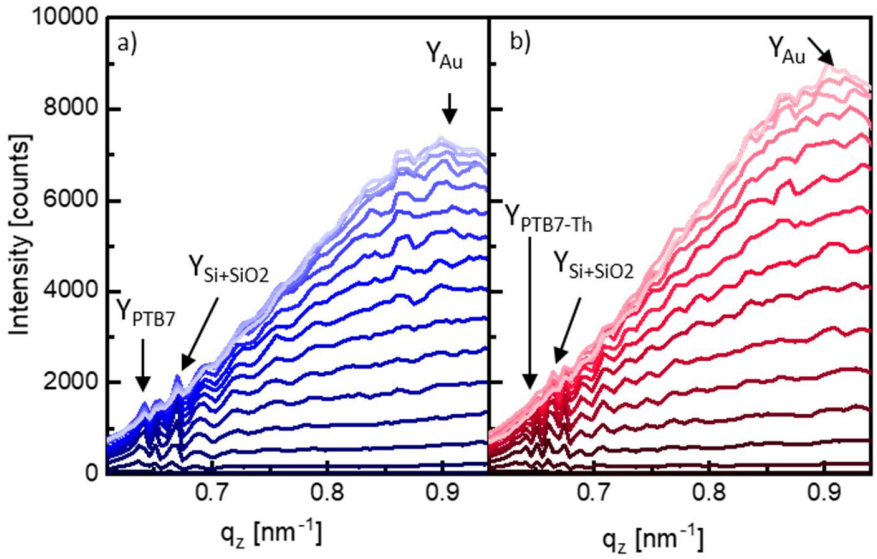

Figure S7: Evolution of the scattering intensity in vertical direction for a) PTB7 and b) PTB7-Th, illustrating the Yoneda peaks of the polymer layer in the first stages (dark curves, peaks at around $q_z \approx 0.66$ to 0.67 nm^{-1}) and the evolution of the strong Yoneda peak intensity of the thin gold layer evolving at $q_z \approx 0.9$ nm^{-1} within the first 30 seconds of sputter deposition. Afterwards, the gold Yoneda peak is partly overlapped by the Kiessig fringes developing due to the growing film thickness.

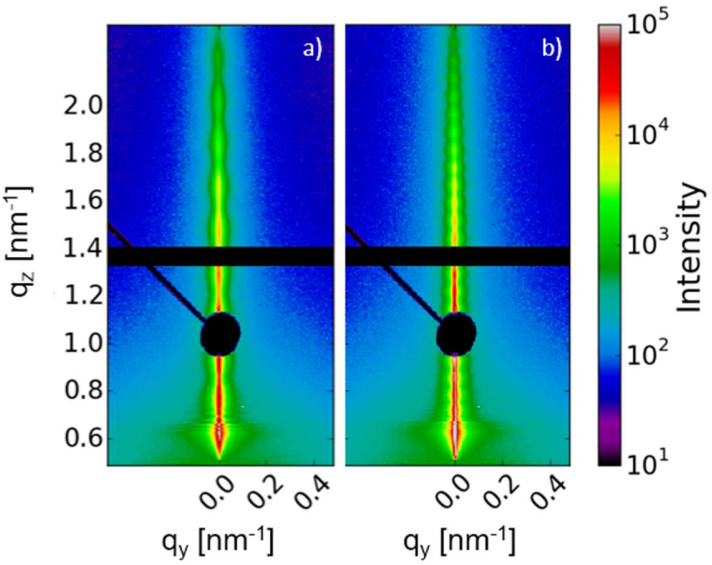

Figure S8: Initial 2D GISAXS data for bare a) PTB7 and b) PTB7-Th thin film, summed up over 11 x 1 second for an improved signal-to-noise ratio.

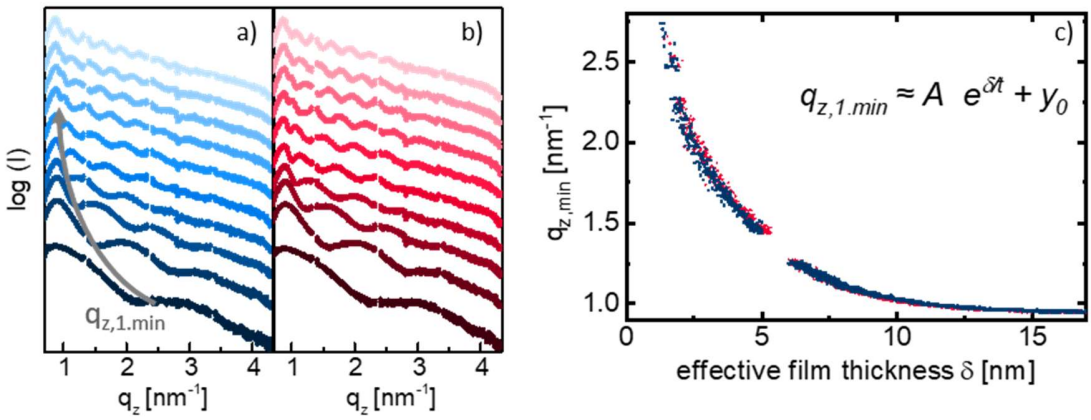

Figure S9: Structure evolution in vertical direction over time illustrated *via* exemplary integrated vertical line (off-detector) cuts of the 2D GISAXS data at 0.1 nm^{-1} < q_y < 2.5 nm^{-1}, taken every 10 seconds starting at t = 10 s for a) PTB7 and b) for PTB7-Th. The intensities are plotted logarithmically for a better visualization of the maxima and shifted along the intensity-axis for clarity. c) Position of the first order minimum $q_{z,1.min}$, as extracted from the off-detector cuts for PTB7 (blue) and PTB7-Th (red), plotted over effective film thickness δ.

Estimation of cluster height *H*:

The first order minimum $q_{z,1.min}$ in the off-detector cuts is directly related to the form factor – and therefore the height H – of the scattering clusters. The evolution of $q_{z,1.min}$ as exponential function of effective film thickness was fitted for both polymers, resulting in A ≈ 2.61 and 2.51, t ≈ 3.02 and 2.97, y_0 ≈ 0.93 and 0.94 for PTB7 and PTB7-Th, respectively. From earlier work by Schwartzkopf et al. (see the corresponding Supporting Information), the simulated $q_{z,min,sim}$ for hemispherical clusters of different heights in a distance of 20 nm are known. (Schwartzkopf et al. 2015) Using the relation $q_{z,1.min,exp}(\delta) = q_{z,min,sim}(H)$ of the fit functions, the cluster height $H(\delta)$ can be extracted for δ < 8 nm.

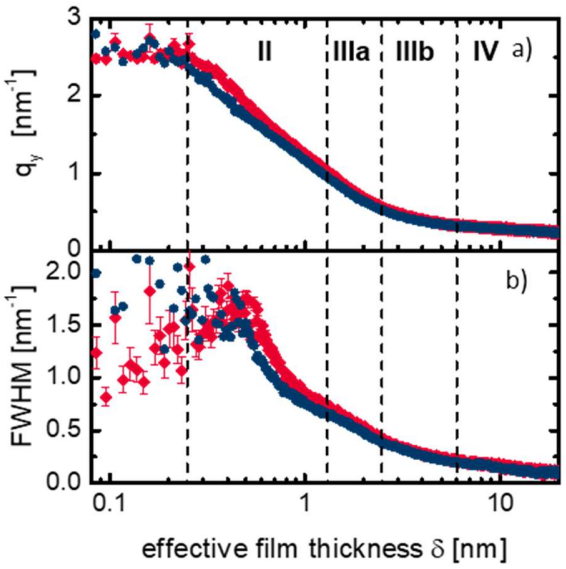

Figure S10: Fitted a) q_y position and b) *FWHM* of the gold side peak in lateral direction for PTB7 (blue) and PTB7-Th (red) over the effective film thickness.

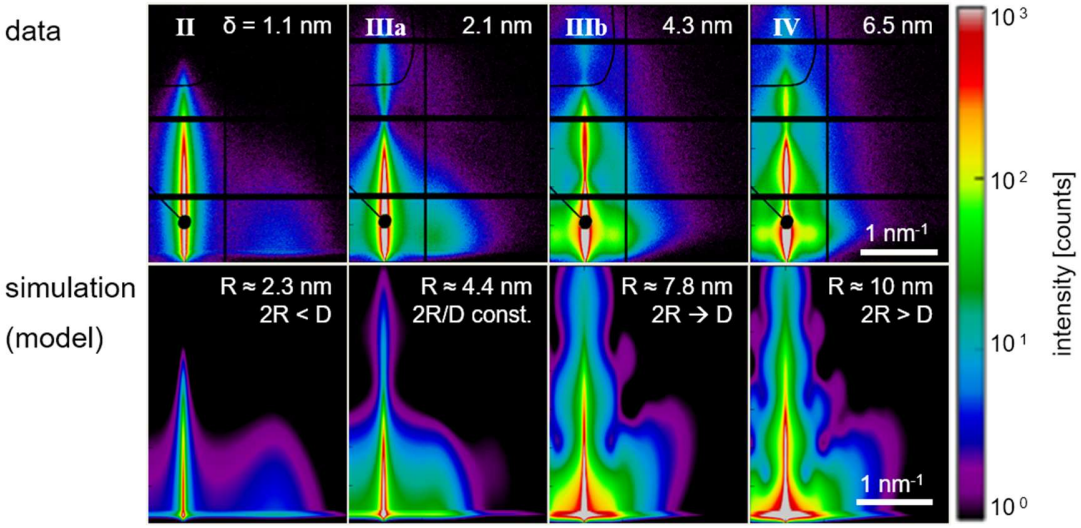

Figure S11: Experimental data for PTB7-Th *vs*. simulated data using the software BornAgain (Burle et al. 2018) and above described model for the different growth phases as indicated with II, IIIa and b, and IV.

Data simulation:

For the modeling of the 2D GISAXS data, the simulation software BornAgain was used. (Burle et al. 2018) Using python scripts, a model of the sample at a specific effective gold film thickness was defined and its theoretical scattering pattern simulated. Here, the model was based on a 2D distribution (1D paracrystalline) of gold clusters (approximated with truncated spheres) with a certain distance and diameter placed onto a polymer film above a silicon substrate. The scattering pattern was simulated using the Distorted Wave Born approximation (DWBA). Deviations from the experimental data are expected, because the modelling was based on the use of simple form factors and structure factors, whereas the real existing nanostructures might be more complex.

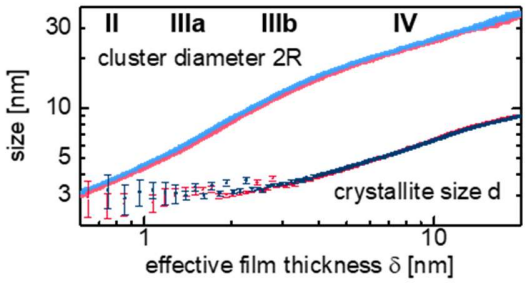

Figure S12: Changes in the minimum gold crystallite size *d* (dark symbols) over effective film thickness δ in comparison to the gold cluster diameter *2R* (light symbols). The minimum crystallite size within the clusters can be determined from the *FWHM* of the (111) Bragg peak in the GIWAXS data using the Scherrer formula. While *2R* is growing quickly even in the very early stages of the deposition process, *d* stays constant during phase II and increases only moderately afterwards.

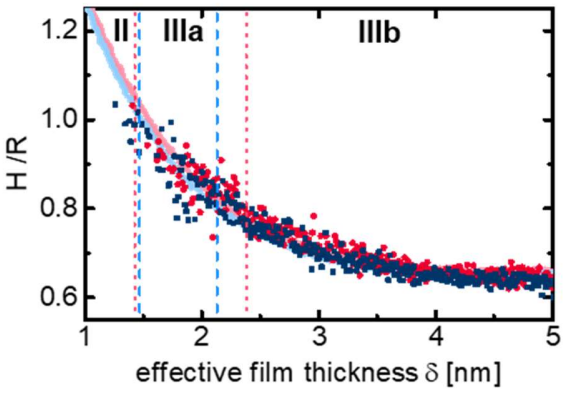

Figure S13: Changes in the *H/R* ratio for PTB7 (dark red) and PTB7-Th (dark blue) over effective film thickness δ, illustrating the change in the form factor of the sputtered gold clusters. The values are extrapolated for smaller δ by calculating H from the fitted $q_{z,min}$ (see Figure S9) and shown in light blue for PTB7 and light red for PTB7-Th. The ratio $H/R \approx 1$ marks the change from phase II to IIIa.

Estimation of the relative surface diffusion coefficient of gold on the respective polymers:

According to the so-called kinetic freezing model by Jeffers et al., the full coalescence of two clusters is hindered when reaching a certain cluster radius, leading to partial coalescence and elongated structures. (Jeffers et al. 1994) The respective critical radius R_c depends on various parameters, such as the metal surface free energy γ, the metal atomic volume Ω, the Boltzmann constant k_B, the deposition rate J and the Temperature T. It is, however, also correlated to the surface diffusion coefficient of the metal on the respective polymer D_s as well as the critical aspect ratio $H/R = \alpha_c$ at the critical effective film thickness δ_c:

$$R_c^4 = \frac{D_s\, \alpha_c\, \delta_c\, \gamma\, \Omega^{4/3}}{k_B\, T\, J}$$

Using the values for R_c, α_c and δ_c from the fitted experimental data at $\delta_c = \delta_{II\text{-}IIIa}$, the relative surface diffusion coefficients for gold on PTB7 and PTB7-Th can be compared via the relation:

$$D_s \sim \frac{R_c^4}{\alpha_c\, \delta_c}$$

The values can additionally be compared to the ones extracted for gold sputter deposited on polystyrene (PS) under the same conditions (sputter setup, sputter rate, temperature, deposition rate, etc.). Even though the critical cluster height was not calculated for Au on PS , we can estimate the H/R ratio to be around or above 1. Using the critical thickness of partial coalescence $\delta_{c,\,PS}$ = 1.6 nm and a critical radius of around 2.8 nm, $D_{s,PS}$ can be estimated to be within the same order of magnitude as PTB7 and PTB7-Th.

Literature

Burle, J.; Durniak, C.; Fisher, J. M.; Ganeva, M.; Pospelov, G.; van Herck, W. et al. (2018): BornAgain - Software for Simulating and Fitting X-Ray and Neutron Small-Angle Scattering at Grazing Incidence. Available online at http://www.bornagainproject.org/, updated on 7/31/2018, checked on 11/27/2019.

Jeffers, G.; Dubson, M. A.; Duxbury, P. M. (1994): Island - to - Percolation Transition During Growth of Metal Films. In *Journal of Applied Physics* 75 (10), pp. 5016–5020. DOI: 10.1063/1.355742.

Jiang, Zhang (2015): GIXSGUI : A MATLAB Toolbox for Grazing-Incidence X-Ray Scattering Data Visualization and Reduction, and Indexing of Buried Three-Dimensional Periodic Nanostructured Films. In *J Appl Crystallogr* 48 (3), pp. 917–926. DOI: 10.1107/S1600576715004434.

Schwartzkopf, Matthias; Santoro, Gonzalo; Brett, Calvin J.; Rothkirch, André; Polonskyi, Oleksandr; Hinz, Alexander et al. (2015): Real-Time Monitoring of Morphology and Optical Properties during Sputter Deposition for Tailoring Metal-Polymer Interfaces. In *ACS Appl. Mater. Interfaces* 7 (24), pp. 13547–13556. DOI: 10.1021/acsami.5b02901.